Vehicle-Grid System Modeling and Stability Analysis With Forbidden Region-Based Criterion

Yicheng Liao, *Student Member, IEEE*, Zhigang Liu, *Senior Member, IEEE*, Guinan Zhang, and Chuan Xiang

***Abstract*—The voltage low frequency oscillation (LFO), between traction network and electric locomotives or electric multiple units in high speed railway, is a typical phenomenon happening in cascade systems with power electronic converters accessed, which is regarded as the stability problem of a vehicle-grid (V2G) system in general. To address the problem, the mathematical model of the V2G system is deduced in detail first, and a generalized *dq*-decoupled small-signal model of a single-phase pulse width modulation rectifier is established in this process. Then, a novel stability criterion based on forbidden region for *dq*-decoupled multi-input multi-output cascade systems is proposed to analyze the stability of the V2G system. The proposed criterion has less conservatism than singular-value criteria and norm criteria, and can be applied for systems with either high or low power factor. The comparison with other criteria and simulation results verifies that the proposed forbidden region-based criterion performs well in the analysis of the critical condition of LFO. Moreover, the impact factors of LFO, both grid parameters and vehicle parameters, are researched based on the proposed stability analysis criterion and the simulation verification, which provides design guidance for the V2G system to restrain LFO.**

***Index Terms*—Cascade system, forbidden region, low frequency oscillation (LFO), pulse width modulation (PWM) rectifier, stability, vehicle-grid (V2G) system.**

I. Introduction

HIGH speed railway (HSR) has been taken into operations more and more widely in recent years. The AC–DC–AC drive system is popularly adopted by electric locomotives and electric multiple units (EMUs) (hereafter called vehicles) in HSR nowadays, which introduces the nonlinearity into the traction power system (TPS) owing to the use of power electronic converters. The safety and stability of TPS are facing more challenges. There have been some low frequency oscillation (LFO) events happening between traction network (hereafter called grid) and vehicles worldwide when multiple vehicles are accessed to the grid [1]. LFOs resulted in traction blockade accidents, which have obstructed the operation of HSR.

Manuscript received February 22, 2016; revised May 25, 2016; accepted June 24, 2016. Date of publication July 7, 2016; date of current version February 2, 2017. This work was supported in part by the National Nature Science Foundation U1434203 and Grant 51377136, and in part by the Sichuan Province Youth Science and Technology Innovation Team 2016TD0012. Recommended for publication by Associate Editor M. Ferdowsi. *(Corresponding author: Zhigang Liu.)*

The authors are with the School of Electrical Engineering, Southwest Jiaotong University, Chengdu 610031, China (e-mail: liaoyichen88@163.com; liuzg_cd@126.com; zgn_2008@126.com; 1091930966@qq.com).

Color versions of one or more of the figures in this paper are available online at http://ieeexplore.ieee.org.

Digital Object Identifier 10.1109/TPEL.2016.2587726

LFO is a phenomenon that the grid voltage or grid current is modulated by, rather than superimposed on a low frequency signal. A study on the fluctuation of the grid voltage by Wang and Wu [2] indicated that the reason for LFO was the insufficiency of the traction substation capacity, while most researchers held the view that the cause for LFO was the mismatching between the electrical parameters of traction network and the control parameters of line-side converters [3]–[5]. Menth *et al.* pointed out that the number of locomotives in operation simultaneously and the control parameters would cause the LFO [4]. Heising *et al.* built a differential equation model of rotary converters as the base of stability analysis for traction power supply system [6], and they demonstrated that using multivariable control could improve the stability of the vehicle-grid (V2G) system [7]. Suarez *et al.* proposed a method to measure the input admittance matrix of the vehicle, and found the critical condition of LFO through stability analysis using Bode diagram [8]. Wang *et al.* built a *dq* model of the V2G system to identify the system as an underdamping one, and made a prediction of the stability by utilizing dominant pole analysis [9].

To sum up, LFO is influenced by both electrical parameters of grid and control parameters of line-side converters, that is to say, LFO is not only power system related, but also power electronics related. The phenomenon of LFO is similar to the unstable phenomenon in other cascade power electronic systems [10], which means that the LFO is actually caused by the cascade structure of a power electronics-based system. As a specific example of power electronics-based systems, the V2G system is a power system–power electronic converter cascade system, which needs deeper research from the perspective of the whole system's stability. However, most of the present researches lack precise mathematical model of the V2G system. Wang *et al.* deduced a mathematical model of vehicle and analyzed LFO on a V2G system comprehensively, but the *dq*-decoupled model of the line-side converter was not a generalized one, and they only used the traditional dominant pole method to analyze the stability, of which the calculation was complicated.

This paper rebuilds the mathematical model of the V2G system and analyzes the stability from the whole system. Since China Railways High-speed 5 (CRH5) EMUs using *dq*-current control are taken for example [9], the grid voltage and current are decoupled into *dq* frames. The V2G system is considered as a multi-input multi-output (MIMO) cascade system.

For the MIMO cascade V2G system, the stability can be analyzed considering the impedance specification, namely the output impedance of the grid and the input admittance of the vehicle. Some different methods were adopted based on impedance

specification, such as singular-value criterion (SVC) [11], [12], norm criterion (NC) [11], [13], and *d*-channel criterion (DCC) [14]–[16]. These methods are simpler than the traditional methods in calculation, such as Nyquist criterion, Bode diagram, dominant pole, etc. However, SVC and NC have certain conservatism in stability analysis, while DCC is only suitable for systems with high power factor. Wen *et al.* [17] proposed a stability analysis method based on forbidden region [18]–[22], which can be classified into DCC to some extent because the coupling variables in *d* and *q* frames are neglected. Taken into account that the power factor of the V2G system is less than one when LFO happens, the coupling variables in *d* and *q* frames cannot be neglected, hence DCC is not suitable for the analysis of LFO. Therefore, this paper proposed a novel stability criterion based on a different forbidden region from [17] to analyze the stability of the system. The proposed criterion is suitable for all kinds of *dq*-decoupled MIMO cascade systems. It not only has less conservatism as compared to SVC and NC, but also can be applied to systems with low power factor. Through the stability analysis and simulation verification, the proposed criterion shows good performance in stability analysis of the V2G system. The factors that may influence LFO could be found, and how they influence the stability could be depicted more precisely.

The rest of this paper is organized as follows: In Section II, the *dq*-decoupled small-signal model of the V2G system is established. In Section III, a novel stability criterion based on forbidden region for a *dq*-decoupled MIMO cascade system is proposed, and the stability of the V2G system with the proposed criterion is analyzed. In Section IV, the simulation and the experiment of LFO in a V2G system is realized to validate the model and the analysis. In Section V, the results of the stability analysis with different criteria and simulation are given and discussed.

This paper analyzes the LFO problem happening in HSR from the perspective of stability analysis of the whole V2G system, which contributes to the stability research on *dq*-decoupled MIMO cascade systems with power electronic converters accessed. On one hand, the generalized *dq*-decoupled small-signal model of single-phase rectifier is established during the mathematical modeling of the V2G system, which may be helpful for the future research on the single-phase rectifiers with *dq*-current control. On the other hand, the proposed forbidden region-based criterion (FRBC) performs better in the stability analysis V2G system than other criteria, and it can also be used in other MIMO cascade systems for the stability analysis. In addition, the impacts on LFO of different parameters are studied more comprehensively than those in [9], which can provide design guidance for restraining LFO.

II. Mathematical Modeling of V2G System

In order to analyze the stability of the V2G system, a precise mathematical model needs to be established first. In the V2G system, the grid is a power system, while the vehicle is a power electronic system, so the model of grid and the model of vehicle should be considered respectively. As the grid and the vehicle are cascaded, the closed-loop transfer function of the whole system can be obtained based on the output impedance of grid and the input admittance of vehicle.

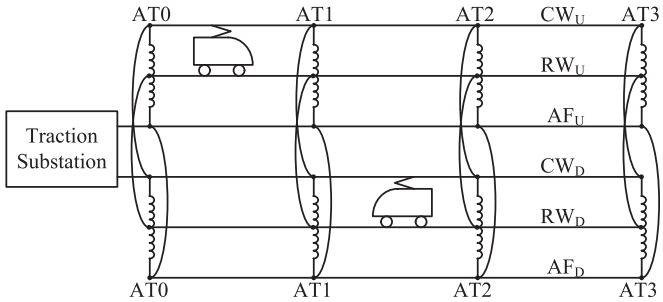

Fig. 1. All-parallel double-tracked AT power supply.

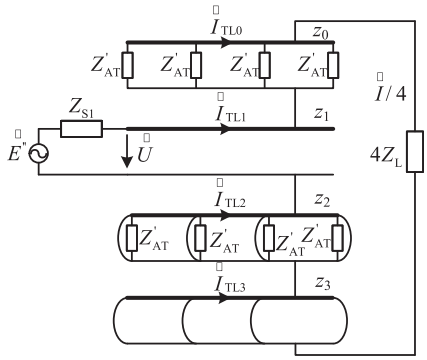

Fig. 2. Equivalent circuit of all-parallel double-tracked AT traction network.

A. Output Impedance of Grid

The output impedance of grid is obtained by deducing the equivalent impedance of traction network. At present, all-parallel double-tracked AT power supply is the main style of the traction network in China, whose diagram is shown in Fig. 1.

The main calculation methods of traction network impedance include equivalent circuit method [23] and generalized method of symmetrical components [24]. Ma proposed a generalized model of symmetrical components considering AT leakage reactance [25]. The equivalent circuit of all-parallel double-tracked AT traction network is shown in Fig. 2, where Z'_{AT} is equal to $2Z_{\mathrm{AT}}$ for the AT leakage reactance is regarded as two reactance of $2Z_{\mathrm{AT}}$ in parallel.

Based on [24], the unit impedance transformation of double-tracked AT traction network is deduced in [25] as

$$\boldsymbol{Z}_{0123} = \boldsymbol{A}_4^{-1}\boldsymbol{Z}_{\mathrm{CW_U\,AF_U\,CW_D\,AF_D}}\boldsymbol{A}_4 \tag{1}$$

where CW and AF denote contact wire and AT feeder, respectively. U and D denote uplink and downlink, respectively. The formula of $\boldsymbol{A}_4$ is

$$\boldsymbol{A}_4 = \begin{bmatrix} 1 & 1 & 1 & 1 \\ 1 & -1 & 1 & -1 \\ 1 & 1 & -1 & -1 \\ 1 & -1 & -1 & 1 \end{bmatrix}. \tag{2}$$

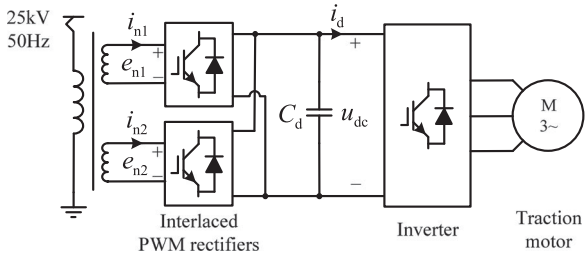

Fig. 3. Each power unit of CRH5 EMUs.

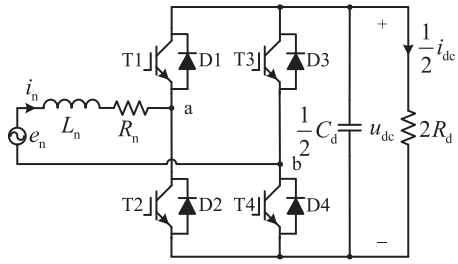

Fig. 4. Equivalent PWM rectifier circuit of each power unit.

From the equivalent circuit in Fig. 2, the equivalent impedance of all-parallel double-tracked AT traction network is deduced as

$$Z_{\mathrm{S}} = \frac{1}{4}\left[\left(z_0 x + Z'_{\mathrm{AT}}\right)\frac{z_0\left(D_{\mathrm{AT}}-x\right)+Z'_{\mathrm{AT}}}{2Z'_{\mathrm{AT}}+z_0 D_{\mathrm{AT}}} + z_1 l + \left(z_2+z_3\right)x\left(1-\frac{x}{D_{\mathrm{AT}}}\right)\right] \tag{3}$$

where x is the distance between the vehicle and the nearest AT station forward, l is the distance between the vehicle and the traction substation, and D_{AT} is the distance between two adjacent AT stations.

B. Input Admittance of Vehicle

The input admittance of vehicle can be obtained by deducing a mathematical model of the vehicle. This paper takes CRH5 EMUs as the example. For the advanced *dq* current control is adopted by CRH5 EMUs [9], the input voltage and current are decoupled into *dq* frames, so the input admittance of CRH5 EMUs is also decoupled into *dq* frames. CRH5 EMUs have five power units and the structure of each power unit [26] is shown in Fig. 3.

In Fig. 3, the input admittance of the vehicle is only determined by the front-end pulse width modulation (PWM) rectifiers. Since each power unit is regarded as two same PWM rectifiers in parallel from the front end, if the input admittance of each PWM rectifier is denoted by $\boldsymbol{Y}_{\mathrm{in}}$, the input admittance of each power unit is $2\boldsymbol{Y}_{\mathrm{in}}$. Assumed that there are *m* vehicles accessed to the traction network and each vehicle has *a* power units, for the power units in one vehicle and different vehicles are all in parallel, the input admittance of all the vehicles can be depicted as

$$\boldsymbol{Y}_{\mathrm{L}} = 2ma\boldsymbol{Y}_{\mathrm{in}} = n\boldsymbol{Y}_{\mathrm{in}}. \tag{4}$$

With the back-end inverters and motors neglected, the load of the two interlaced rectifiers can be equivalent to a constant resistance R_{d}. The equivalent circuit of each rectifier is shown in Fig. 4, where L_{n} and R_{n} are the equivalent inductance and resistance respectively of the secondary winding of the traction transformer, and C_{d} is the DC-link capacitor of the two interlaced rectifiers. Since C_{d} and R_{d} are supplied by the two same rectifiers in parallel, for each rectifier, the load current is half of that for double rectifiers. The equivalent capacitor and load for a single rectifier are $1/2C_{\mathrm{d}}$ and $2R_{\mathrm{d}}$, respectively.

Assumed that d_{a} and d_{b} denote the switch states of leg a and leg b, respectively, the relationships among the input voltage e_{n}, the input current i_{n}, and the DC-link voltage u_{dc} are

$$\begin{cases} L_{\mathrm{n}}\frac{\mathrm{d}i_{\mathrm{n}}}{\mathrm{d}t} = e_{\mathrm{n}} - i_{\mathrm{n}}R_{\mathrm{n}} - \left(d_{\mathrm{a}}-d_{\mathrm{b}}\right)u_{\mathrm{dc}} \\ \frac{1}{2}C_{\mathrm{d}}\frac{\mathrm{d}u_{\mathrm{dc}}}{\mathrm{d}t} = \left(d_{\mathrm{a}}-d_{\mathrm{b}}\right)i_{\mathrm{n}} - \frac{u_{\mathrm{dc}}}{2R_{\mathrm{d}}} \end{cases}. \tag{5}$$

Since *dq* current control is adopted, the input voltage e_{n} and the input current i_{n} need to be decoupled into *dq* frames, which are e_d, e_q, and i_d, i_q. As we all know, the *dq* components are obtained from the $\alpha\beta$ components via Park transformation, which is shown as

$$T_{\alpha\beta-dq} = \begin{bmatrix} \cos\omega t & \sin\omega t \\ -\sin\omega t & \cos\omega t \end{bmatrix} \tag{6}$$

where ωt is the locked phase of the input voltage e_{n}.

In the single-phase rectifier, if e_{n} and i_{n} are regarded as components in α frame, there are no actual components in the β frame. Therefore, the imaginary voltage and current in the β frame are fabricated as 90° lagging behind the α components so that (6) will make sense [27]. Through the inverse transformation of (6), it follows that

$$v_\alpha = v_d\cos\omega t - v_q\sin\omega t, \tag{7}$$

where *v* denotes the corresponding variable.

Supposed that $e_{\mathrm{n}} = e_\alpha$, $i_{\mathrm{n}} = i_\alpha$, $d_{\mathrm{a}} - d_{\mathrm{b}} = d_\alpha$, and substituting (7), (5) can be decoupled into *dq* frames as

$$\begin{cases} L_{\mathrm{n}}\frac{\mathrm{d}i_d}{\mathrm{d}t} = e_d - i_dR_{\mathrm{n}} + \omega L_{\mathrm{n}}i_q - d_du_{\mathrm{dc}} \\ L_{\mathrm{n}}\frac{\mathrm{d}i_q}{\mathrm{d}t} = e_q - i_qR_{\mathrm{n}} - \omega L_{\mathrm{n}}i_d - d_qu_{\mathrm{dc}} \\ \frac{1}{2}C_{\mathrm{d}}\frac{\mathrm{d}u_{\mathrm{dc}}}{\mathrm{d}t} \approx \frac{1}{2}\left(d_di_d + d_qi_q\right) - \frac{u_{\mathrm{dc}}}{2R_{\mathrm{d}}} \end{cases} \tag{8}$$

where the third equation is obtained with an approximation for the product of d component and q component is very small. Therefore, the equivalent *dq*-decoupled circuit of Fig. 4 can be obtained as shown in Fig. 5 according to (8). i_M is the equivalent current at DC-link.

At the fixed point, with capital letters, (8) can be depicted as

$$\begin{cases} 0 = E_d - I_dR_{\mathrm{n}} + \omega L_{\mathrm{n}}I_q - D_dU_{\mathrm{dc}} \\ 0 = E_q - I_qR_{\mathrm{n}} - \omega L_{\mathrm{n}}I_d - D_qU_{\mathrm{dc}} \\ 0 = \frac{1}{2}\left(D_dI_d + D_qI_q\right) - \frac{U_{\mathrm{dc}}}{2R_{\mathrm{d}}} \end{cases}. \tag{9}$$

Since ωt is the locked phase of the input voltage e_{n}, through Park transformation, it follows that e_q is equal to zero, so does E_q. E_d is equal to the amplitude of e_{n}. The PWM rectifier is required to work under unit power factor, so I_q is also equal

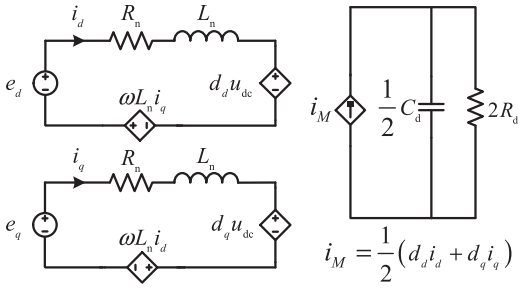

Fig. 5. Equivalent *dq*-decoupled circuit of the PWM rectifier.

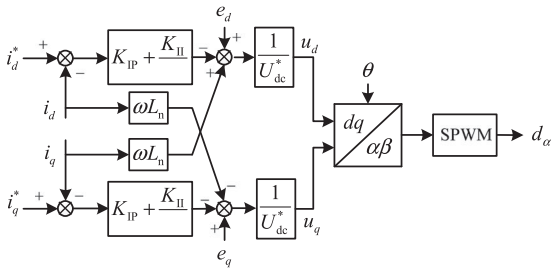

Fig. 6. *dq* current control of CRH5 EMUs' PWM rectifier.

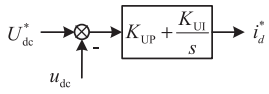

Fig. 7. Voltage loop control of CRH5 EMUs' PWM rectifier.

to zero. Then, given the values of E_d and $U_{\rm dc}$, the steady-state values of I_d, D_d, and D_q can be obtained from (9), as shown below

$$\begin{cases} I_d = \frac{E_d - \sqrt{E_d^2 - \frac{4R_{\rm n}}{R_{\rm d}}U_{\rm dc}^2}}{2R_{\rm n}} \\ D_d = \frac{R_{\rm n}U_{\rm dc}}{R_{\rm d}\left(E_d - \sqrt{E_d^2 - \frac{4R_{\rm n}}{R_{\rm d}}U_{\rm dc}^2}\right)} \\ D_q = -\frac{\omega L_{\rm n}\left(E_d - \sqrt{E_d^2 - \frac{4R_{\rm n}}{R_{\rm d}}U_{\rm dc}^2}\right)}{2R_{\rm n}U_{\rm dc}} \end{cases}. \tag{10}$$

In order to deduce the small-signal model of the rectifier, each variable in (8) is regarded as a steady-state value plus a small-signal value. Equation (8) can be rewritten as

$$\begin{cases} L_{\rm n}\frac{{\rm d}\left(I_d+\hat{i}_d\right)}{{\rm d}t} = E_d + \hat{e}_d - \left(I_d + \hat{i}_d\right)R_{\rm n} + \omega L_{\rm n}\left(I_q + \hat{i}_q\right) \\ \qquad - \left(D_d + \hat{d}_d\right)\left(U_{\rm dc} + \hat{u}_{\rm dc}\right) \\ L_{\rm n}\frac{{\rm d}\left(I_q+\hat{i}_q\right)}{{\rm d}t} = E_q + \hat{e}_q - \left(I_q + \hat{i}_q\right)R_{\rm n} - \omega L_{\rm n}\left(I_d + \hat{i}_d\right) \\ \qquad - \left(D_q + \hat{d}_q\right)\left(U_{\rm dc} + \hat{u}_{\rm dc}\right) \\ \frac{1}{2}C_{\rm d}\frac{{\rm d}(U_{\rm dc}+\hat{u}_{\rm dc})}{{\rm d}t} = \frac{1}{2}\left(D_d + \hat{d}_d\right)\left(I_d + \hat{i}_d\right) \\ \qquad + \frac{1}{2}\left(D_q + \hat{d}_q\right)\left(I_q + \hat{i}_q\right) - \frac{U_{\rm dc}+\hat{u}_{\rm dc}}{2R_{\rm d}} \end{cases} \tag{11}$$

where the variables with hats denote the corresponding small-signal values.

With the steady-state values and the infinitesimal values of two small-signal values' product omitted, the *dq*-decoupled small-signal model of the rectifier in matrix form can be obtained as

$$\begin{aligned} \frac{\rm d}{{\rm d}t}\begin{bmatrix} \hat{i}_d \\ \hat{i}_q \\ \hat{u}_{\rm dc} \end{bmatrix} &= \begin{bmatrix} -\frac{R_{\rm n}}{L_{\rm n}} & \omega & -\frac{D_d}{L_{\rm n}} \\ -\omega & -\frac{R_{\rm n}}{L_{\rm n}} & -\frac{D_q}{L_{\rm n}} \\ \frac{D_d}{C_{\rm d}} & \frac{D_q}{C_{\rm d}} & -\frac{1}{C_{\rm d}R_{\rm d}} \end{bmatrix}\begin{bmatrix} \hat{i}_d \\ \hat{i}_q \\ \hat{u}_{\rm dc} \end{bmatrix} \\ &\quad + \begin{bmatrix} -\frac{U_{\rm dc}}{L_{\rm n}} & 0 \\ 0 & -\frac{U_{\rm dc}}{L_{\rm n}} \\ \frac{I_d}{C_{\rm d}} & \frac{I_q}{C_{\rm d}} \end{bmatrix}\begin{bmatrix} \hat{d}_d \\ \hat{d}_q \end{bmatrix} + \begin{bmatrix} \frac{1}{L_{\rm n}} & 0 \\ 0 & \frac{1}{L_{\rm n}} \\ 0 & 0 \end{bmatrix}\begin{bmatrix} \hat{e}_d \\ \hat{e}_q \end{bmatrix} \\ &= \boldsymbol{A}\begin{bmatrix} \hat{i}_d \\ \hat{i}_q \\ \hat{u}_{\rm dc} \end{bmatrix} + \boldsymbol{B}\begin{bmatrix} \hat{d}_d \\ \hat{d}_q \end{bmatrix} + \boldsymbol{C}\begin{bmatrix} \hat{e}_d \\ \hat{e}_q \end{bmatrix} \end{aligned} \tag{12}$$

where $\boldsymbol{A}$, $\boldsymbol{B}$, and $\boldsymbol{C}$ are the corresponding coefficient matrixes.

Laplace transformation is applied to (12), resulting in

$$\begin{bmatrix} \hat{i}_d \\ \hat{i}_q \\ \hat{u}_{\rm dc} \end{bmatrix} = (s\boldsymbol{I}_3 - \boldsymbol{A})^{-1}\boldsymbol{B}\begin{bmatrix} \hat{d}_d \\ \hat{d}_q \end{bmatrix} + (s\boldsymbol{I}_3 - \boldsymbol{A})^{-1}\boldsymbol{C}\begin{bmatrix} \hat{e}_d \\ \hat{e}_q \end{bmatrix}, \tag{13}$$

where $\boldsymbol{I}_3$ is a three by three unit matrix.

Equation (13) illustrates a generalized *dq*-decoupled small-signal model of single phase PWM rectifier. $\hat{d}_d$ and $\hat{d}_q$ vary from different control strategies. The diagram of *dq* current control [28] adopted by CRH5 EMUs is shown in Fig. 6.

From Fig. 6, it follows that:

$$\begin{cases} u_d = \frac{1}{U_{\rm dc}^*}\left[e_d - \left(i_d^* - i_d\right)H_{\rm I} + i_q\omega L_{\rm n}\right] \\ u_q = \frac{1}{U_{\rm dc}^*}\left[e_q - \left(i_q^* - i_q\right)H_{\rm I} - i_d\omega L_{\rm n}\right] \end{cases} \tag{14}$$

where i_q^* is equal to zero, and i_d^* can be obtained by the voltage loop control shown in Fig. 7. $U_{\rm dc}^*$ is the reference of DC-link voltage. $H_{\rm I}$ is the transfer function of the proportional-integral (PI) controller in the current loop, which is

$$H_{\rm I} = K_{\rm IP} + \frac{K_{\rm II}}{s}. \tag{15}$$

From Fig. 7, i_d^* can be depicted as

$$i_d^* = \left(U_{\rm dc}^* - u_{\rm dc}\right)H_{\rm U} \tag{16}$$

where $H_{\rm U}$ is the transfer function of the PI controller in the voltage loop, which is

$$H_{\rm U} = K_{\rm UP} + \frac{K_{\rm UI}}{s}. \tag{17}$$

The sinusoidal pulse width modulation (SPWM) in Fig. 6 could be mapped to *dq* frames. $[d_d, d_q]^{\rm T}$ is obtained through a SPWM from $[u_d, u_q]^{\rm T}$ directly. Assumed that the amplitude of the carrier wave is $U_{\rm C}$, the relationship between $[d_d, d_q]^{\rm T}$ and

$[u_d, u_q]^{\mathrm{T}}$ is

$$\begin{bmatrix} d_d \\ d_q \end{bmatrix} = \frac{1}{2U_{\mathrm{C}}} \begin{bmatrix} u_d \\ u_q \end{bmatrix} = \frac{1}{2} \begin{bmatrix} u_d \\ u_q \end{bmatrix} \tag{18}$$

where U_{C} is equal to one because of the normalization.

Combining (14), (16), and (18), it can be derived that

$$\begin{aligned} \begin{bmatrix} \hat{d}_d \\ \hat{d}_q \end{bmatrix} &= \begin{bmatrix} \frac{H_{\mathrm{I}}}{2U_{\mathrm{dc}}^*} & \frac{\omega L_{\mathrm{n}}}{2U_{\mathrm{dc}}^*} & \frac{H_{\mathrm{I}} H_{\mathrm{U}}}{2U_{\mathrm{dc}}^*} \\ -\frac{\omega L_{\mathrm{n}}}{2U_{\mathrm{dc}}^*} & \frac{H_{\mathrm{I}}}{2U_{\mathrm{dc}}^*} & 0 \end{bmatrix} \begin{bmatrix} \hat{i}_d \\ \hat{i}_q \\ \hat{u}_{\mathrm{dc}} \end{bmatrix} + \begin{bmatrix} \frac{1}{2U_{\mathrm{dc}}^*} & \\ & \frac{1}{2U_{\mathrm{dc}}^*} \end{bmatrix} \\ &\quad \times \begin{bmatrix} \hat{e}_d \\ \hat{e}_q \end{bmatrix} \\ &= \boldsymbol{D} \begin{bmatrix} \hat{i}_d \\ \hat{i}_q \\ \hat{u}_{\mathrm{dc}} \end{bmatrix} + \boldsymbol{E} \begin{bmatrix} \hat{e}_d \\ \hat{e}_q \end{bmatrix} \end{aligned} \tag{19}$$

where $\boldsymbol{D}$ and $\boldsymbol{E}$ are the corresponding coefficient matrixes.

Substituting (19) into (13), it follows that

$$\begin{aligned} \begin{bmatrix} \hat{i}_d \\ \hat{i}_q \\ \hat{u}_{\mathrm{dc}} \end{bmatrix} &= \left[\boldsymbol{I}_3 - (s\boldsymbol{I}_3 - \boldsymbol{A})^{-1}\boldsymbol{B}\boldsymbol{D}\right]^{-1} (s\boldsymbol{I}_3 - \boldsymbol{A})^{-1} \\ &\quad \times (\boldsymbol{B}\boldsymbol{E} + \boldsymbol{C}) \begin{bmatrix} \hat{e}_d \\ \hat{e}_q \end{bmatrix} \\ &= \boldsymbol{G}_{iu-e} \begin{bmatrix} \hat{e}_d \\ \hat{e}_q \end{bmatrix} = \begin{bmatrix} \boldsymbol{G}_{i-e} \\ \boldsymbol{G}_{u\text{-}e} \end{bmatrix} \begin{bmatrix} \hat{e}_d \\ \hat{e}_q \end{bmatrix} \end{aligned} \tag{20}$$

where $\boldsymbol{G}_{iu-e}$ is defined as the transfer matrix from $[\hat{e}_d, \hat{e}_q]^{\mathrm{T}}$ to $[\hat{i}_d, \hat{i}_q, \hat{u}_{\mathrm{dc}}]^{\mathrm{T}}$. G_{i-e} is a two by two block matrix and $\boldsymbol{G}_{u-e}$ is a one by two block matrix.

Thus, the input admittance of the single PWM rectifier can be depicted as

$$\boldsymbol{Y}_{\mathrm{in}} = \frac{\hat{\boldsymbol{i}}}{\hat{\boldsymbol{e}}} = \boldsymbol{G}_{i-e}. \tag{21}$$

From (4) and (21), the total input admittance of the vehicles is a matrix in *dq* frames, which is depicted as

$$\boldsymbol{Y}_{\mathrm{L}dq} = 2ma\boldsymbol{Y}_{\mathrm{in}} = n\boldsymbol{Y}_{\mathrm{in}}. \tag{22}$$

C. Transfer Function Matrix of V2G System

Since the input admittance of vehicles is decoupled into *dq* frames as $\boldsymbol{Y}_{\mathrm{L}dq}$, the output impedance of grid should also be decoupled into *dq* frames, which is

$$\boldsymbol{Z}_{\mathrm{S}dq} = \begin{bmatrix} R_{\mathrm{s}} + sL_{\mathrm{s}} & -\omega L_{\mathrm{s}} \\ \omega L_{\mathrm{s}} & R_{\mathrm{s}} + sL_{\mathrm{s}} \end{bmatrix} \tag{23}$$

where the values of the grid resistance and inductance need to be converted to the secondary side of the traction transformer. Thus, the V2G system can be considered as a MIMO cascade system, as shown in Fig. 8. From Kirchhoff's voltage law, the relationship between $\boldsymbol{e}_{\mathrm{S}}$ and $\boldsymbol{i}_{\mathrm{L}}$ is

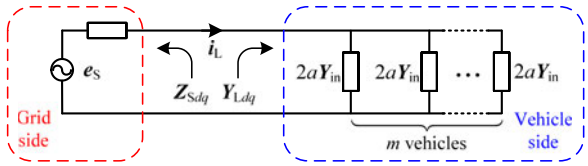

Fig. 8. Topological graph of V2G cascaded system.

$$\boldsymbol{e}_{\mathrm{S}} - \boldsymbol{Z}_{\mathrm{S}dq}\boldsymbol{i}_{\mathrm{L}} = \boldsymbol{Y}_{\mathrm{L}dq}^{-1}\boldsymbol{i}_{\mathrm{L}}. \tag{24}$$

Then the closed-loop transfer function matrix of the V2G system from $\boldsymbol{e}_{\mathrm{S}}$ to $\boldsymbol{i}_{\mathrm{L}}$ can be deduced from (24) as

$$\boldsymbol{G}_{\mathrm{cl}} = \boldsymbol{Y}_{\mathrm{L}dq}(\boldsymbol{I}_2 + \boldsymbol{Z}_{\mathrm{S}dq}\boldsymbol{Y}_{\mathrm{L}dq})^{-1} = \boldsymbol{Y}_{\mathrm{L}dq}(\boldsymbol{I}_2 + \boldsymbol{L}_{dq})^{-1} \tag{25}$$

where $\boldsymbol{I}_2$ is a two by two unit matrix. The return-ratio matrix is defined as

$$\boldsymbol{L}_{dq} = \boldsymbol{Z}_{\mathrm{S}dq}\boldsymbol{Y}_{\mathrm{L}dq}. \tag{26}$$

III. Stability Analysis of V2G System

Since the closed-loop transfer function matrix of the V2G system is derived, the stability can be analyzed. For the MIMO cascade system, the traditional stability analysis methods are Generalized Nyquist Criterion (GNC) and Bode diagram, but they are relatively more complicated than the later proposed criteria, such as SVC and NC. However, the SVC and NC are used with some conservatism. Therefore, the FRBC with less conservatism is put forward in this section. With the FRBC, the stability of a V2G system is analyzed on magnitude-frequency diagram, which is clear and direct, and the critical unstable number of vehicles can be obtained.

A. SVC and NC for dq-Decoupled MIMO Cascade System

For the *dq*-decoupled MIMO cascade system, the output impedance of the front subsystem and the input admittance of the after subsystem are assumed as

$$\boldsymbol{Z}_{\mathrm{S}dq} = \begin{bmatrix} Z_{dd} & Z_{dq} \\ Z_{qd} & Z_{qq} \end{bmatrix} \tag{27}$$

$$\boldsymbol{Y}_{\mathrm{L}dq} = \begin{bmatrix} Y_{dd} & Y_{dq} \\ Y_{qd} & Y_{qq} \end{bmatrix}. \tag{28}$$

Then, the return-ratio matrix is

$$\boldsymbol{L}_{dq} = \boldsymbol{Z}_{\mathrm{S}dq}\boldsymbol{Y}_{\mathrm{L}dq} = \begin{bmatrix} Z_{dd} & Z_{dq} \\ Z_{qd} & Z_{qq} \end{bmatrix} \begin{bmatrix} Y_{dd} & Y_{dq} \\ Y_{qd} & Y_{qq} \end{bmatrix} = \begin{bmatrix} L_{dd} & L_{dq} \\ L_{qd} & L_{qq} \end{bmatrix}. \tag{29}$$

Given the closed-loop transfer function as (25), according to GNC, the system is closed-loop stable if and only if the sum of anti-clockwise encirclements of the critical point $(-1+j0)$

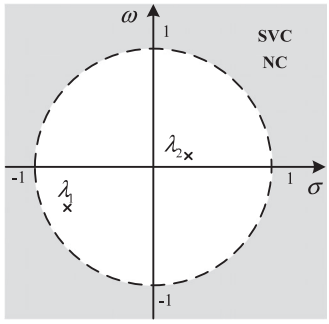

Fig. 9. Distribution limitation of the eigenvalues of $\boldsymbol{L}_{dq}$ for MISC, SVC and NC.

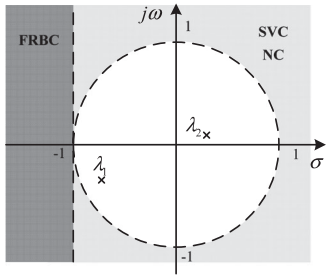

Fig. 10. Reduced forbidden region of FRBC for MIMO cascade system.

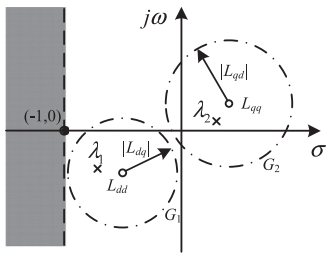

Fig. 11. Relationship between the forbidden region of FRBC and the GDs of $\boldsymbol{L}_{dq}$.

by all the eigenvalues λ_i of $\boldsymbol{L}_{dq}$ is equal to the number of right-half complex plane poles of $\boldsymbol{L}_{dq}$ [29]. The vehicle and the grid subsystems are stable separately, that is to say, the poles in the right-half complex plane of $\boldsymbol{Z}_{\mathrm{S}dq}$ and of $\boldsymbol{Y}_{\mathrm{L}dq}$ are zero, respectively. Hence, the stable condition of the V2G system is that the sum of anti-clockwise encirclements of the critical point $(-1+j0)$ by all the eigenvalues λ_i of $\boldsymbol{L}_{dq}$ is zero.

Middlebrook's impedance stability criterion (MISC) [30] can be generalized in MIMO cascade system, namely, the system is stable when all the eigenvalues of $\boldsymbol{L}_{dq}$ are in a unit circle around the origin, as shown in Fig. 9. The SVC and NC proposed in [11]–[13] are all based on MISC, which are shown in (30) and (31) respectively.

The SVC in [11] and [12] is

$$\bar{\sigma}\left(\boldsymbol{Z}_{\mathrm{S}dq}\right)\cdot\bar{\sigma}\left(\boldsymbol{Y}_{\mathrm{L}dq}\right)<1 \tag{30}$$

where $\bar{\sigma}$ denotes the maximum singular value of the matrix.

The NC advanced by Liu *et al.* [13] is

$$\left(\left\|\boldsymbol{Z}_{\mathrm{S}dq}\right\|_{\mathrm{G}}\cdot\left\|\boldsymbol{Y}_{\mathrm{L}dq}\right\|_{\mathrm{sum}}<1\right)\cup\left(\left\|\boldsymbol{Y}_{\mathrm{L}dq}\right\|_{\mathrm{G}}\cdot\left\|\boldsymbol{Z}_{\mathrm{S}dq}\right\|_{\mathrm{sum}}<1\right) \tag{31}$$

where the G-norm and sum-norm are defined as

$$\|\boldsymbol{A}\|_{\mathrm{G}}=\max_{i,j}|a_{ij}| \tag{32}$$

$$\|\boldsymbol{A}\|_{\mathrm{sum}}=\sum_{i,j}|a_{ij}|. \tag{33}$$

However, the constraint of the eigenvalues inside the unit circle around the origin makes the SVC and NC be sufficient conditions, which leads to certain conservatism of the stability analysis. The conservatism shows the degree of the sufficiency.

B. FRBC for dq-Decoupled MIMO Cascade System

If the region outside the unit circle around the origin is regarded as the forbidden region of the eigenvalues of $\boldsymbol{L}_{dq}$ in Fig. 9, then the conservatism can be decreased by reducing the forbidden region. In contrast to Fig. 9, the forbidden region is reduced to the left side of $(-1+j0)$, as shown in Fig. 10, which can still ensure the zero contour number of the eigenvalues of $\boldsymbol{L}_{dq}$ around $(-1+j0)$.

In order to limit the distribution area of the eigenvalues of $\boldsymbol{L}_{dq}$, Gerschogorin Disc Theorem (GDT) is used to estimate the eigenvalues of a matrix. From GDT [31], the eigenvalue of a matrix locates in a circle around the diagonal element, with a radius of the sum of nondiagonal elements' modules in the same row. Thus, the eigenvalue λ_i of $\boldsymbol{L}_{dq}$ locates in the Gerschogorin disc (GD) G_1 or G_2 in Fig. 11, which conforms to

$$|\lambda_i-L_{dd}|<|L_{dq}|\ \text{ or }\ |\lambda_i-L_{qq}|<|L_{qd}|. \tag{34}$$

From (34) and Fig. 11, the sufficient stable condition of the system is

$$\begin{cases}\mathrm{Re}\left\{L_{dd}\right\}-|L_{dq}|>-1\\ \mathrm{Re}\left\{L_{qq}\right\}-|L_{qd}|>-1\end{cases}. \tag{35}$$

On the other hand, for $\boldsymbol{L}_{dq}^{\mathrm{T}}$ and $\boldsymbol{L}_{dq}$ have the same eigenvalues, all the eigenvalues of $\boldsymbol{L}_{dq}$ are also in the GDs of $\boldsymbol{L}_{dq}^{\mathrm{T}}$, which are the column GDs of $\boldsymbol{L}_{dq}$. Thus, the relationship is obtained as follows:

$$|\lambda_i-L_{dd}|<|L_{qd}|\ \text{ or }\ |\lambda_i-L_{qq}|<|L_{dq}|. \tag{36}$$

It is followed from (36) that the sufficient stable condition of the system is:

$$\begin{cases}\mathrm{Re}\left\{L_{dd}\right\}-|L_{qd}|>-1\\ \mathrm{Re}\left\{L_{qq}\right\}-|L_{dq}|>-1\end{cases}. \tag{37}$$

All the eigenvalues of $\boldsymbol{L}_{dq}$ are located in the intersection of the GDs and the column GDs of $\boldsymbol{L}_{dq}$, which is the satisfaction region for the stable system. Hence, the rejection region for the stable system is the union of the rejection regions for (35) and (37). However, there are still some stable systems' eigenvalues located in the rejection regions for (35) and (37) on account of the sufficiency of the condition. The rejection region for the

TABLE I
PARAMETERS OF V2G SYSTEM (CASE 1)

Parameters	Values	Parameters	Values
E_{S}	27.5 kV	C_{d}	9 mF
R_{S}	0.2 Ω	R_{d}	25 Ω
L_{S}	6 mH	K_{UP}	0.5
R_{n}	0.145 Ω	K_{UI}	5
L_{n}	5.4 mH	K_{IP}	2
U_{dc}	3600 V	K_{II}	50

stable system could be reduced to the intersection of the rejection regions for (35) and (37). Thus, the satisfaction region for the stable system can be expanded to the union of the rejection regions for (35) and (37), which further decreases the conservatism. The obtained criterion for a stable system is

$$\left(\begin{cases}\mathrm{Re}\{L_{dd}\}-|L_{dq}|+1>0\\ \mathrm{Re}\{L_{qq}\}-|L_{qd}|+1>0\end{cases}\right)\cup\left(\begin{cases}\mathrm{Re}\{L_{dd}\}-|L_{qd}|+1>0\\ \mathrm{Re}\{L_{qq}\}-|L_{dq}|+1>0\end{cases}\right) \tag{38}$$

where the four subcriteria are

$$\mathrm{Re}\{L_{dd}\}-|L_{dq}|+1>0 \tag{38a}$$
$$\mathrm{Re}\{L_{qq}\}-|L_{qd}|+1>0 \tag{38b}$$
$$\mathrm{Re}\{L_{dd}\}-|L_{qd}|+1>0 \tag{38c}$$
$$\mathrm{Re}\{L_{qq}\}-|L_{dq}|+1>0. \tag{38d}$$

C. Stability Analysis With FRBC

With the proposed FRBC, the stability of the V2G system can be analyzed. Proper parameters are selected to analyze the stability of the V2G system, as shown in Table I (Case 1). The impedance of grid is approximately calculated with (3), for the accurate impedance is not able to be obtained. The electrical parameters of CRH5 EMUs are considered as designed in the actual products, and the control parameters are determined through the simulation in the next section.

The proposed criterion shown in (38) can be depicted on a magnitude-frequency diagram, as shown in Fig. 12, which displays the stability analyses when one, seven, and eight vehicles are put into operation, respectively. The four lines, two blue lines and two red lines, denote the four subcriteria respectively, as shown in the legend of the figures. According to (38), the system is stable if both of the blue lines or both of the red lines are above zero.

In Fig. 12(a), all the four lines are above zero, thus the system with one vehicle accessed is stable. As the number of vehicles increases to seven, in Fig. 12(b), although the lowest point of the blue solid line is below zero, both the red lines are still above zero, so the system is also stable. But in Fig. 12(c), the lowest points of the red dotted line and of the blue solid line are both below zero, which indicates that the system becomes unstable when the eighth vehicle is accessed to the grid. Thus, it is found that the critical unstable number of vehicles under Case 1 is eight.

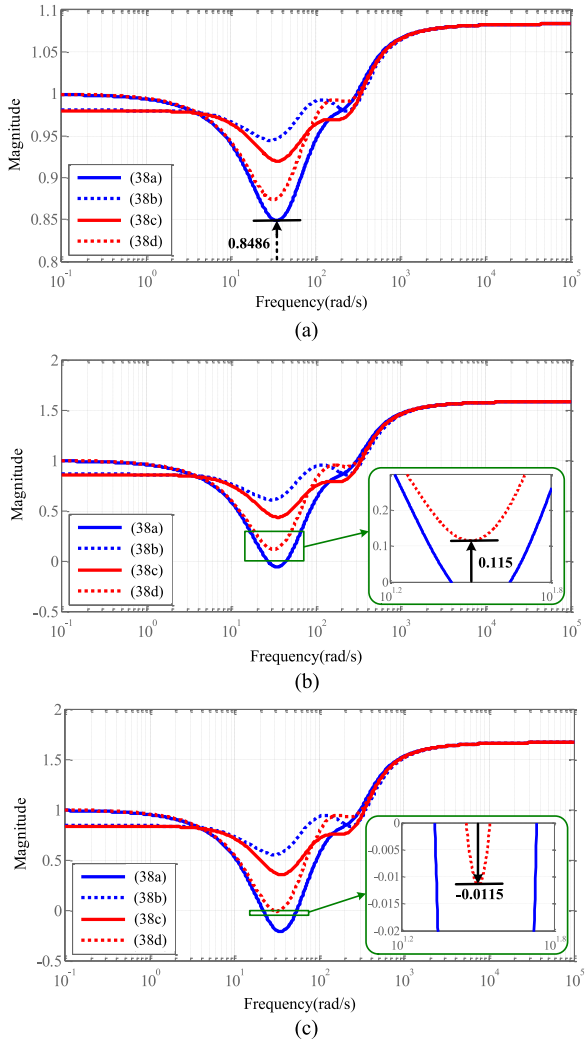

Fig. 12. Stability analyses with FBRC under Case 1. (a) One vehicle accessed to the grid: stable. (b) Seven vehicles accessed to the grid: stable. (c) Eight vehicles accessed to the grid: unstable.

According to (29) and (38), $\boldsymbol{Z}_{\mathrm{S}dq}$ and $\boldsymbol{Y}_{\mathrm{L}dq}$ play important roles in the stability of the V2G system, which are related to the grid parameters and the vehicle parameters respectively. The influences of grid parameters and vehicle parameters are analyzed through the stability analyses with FRBC respectively.

1) Influence of Grid Parameters: The resistance R_{S} and inductance L_{S} of the traction network are the main factors of $\boldsymbol{Z}_{\mathrm{S}dq}$ according to (23). Fig. 13 displays the stability analyses with FRBC when R_{S} changes under Case 1. Compared with Fig. 12(c), Fig. 13(a) shows that when R_{S} increases, the V2G system with eight vehicles accessed becomes stable from unstable. In Fig. 13(b), when R_{S} decreases, the V2G system with seven vehicles accessed is still stable in contrast to Fig. 12(b). But from the enlarged views, the lowest point of the red dotted line in Fig. 12(b) is 0.115 above zero, while that in Fig. 13(b) is 0.1011 above zero. It indicates that the decrease of R_S will destabilize the V2G system even if it does not cause apparent change of stability in vehicle number. As a result, it is found that larger R_{S} benefits the stability of the whole system, but whose

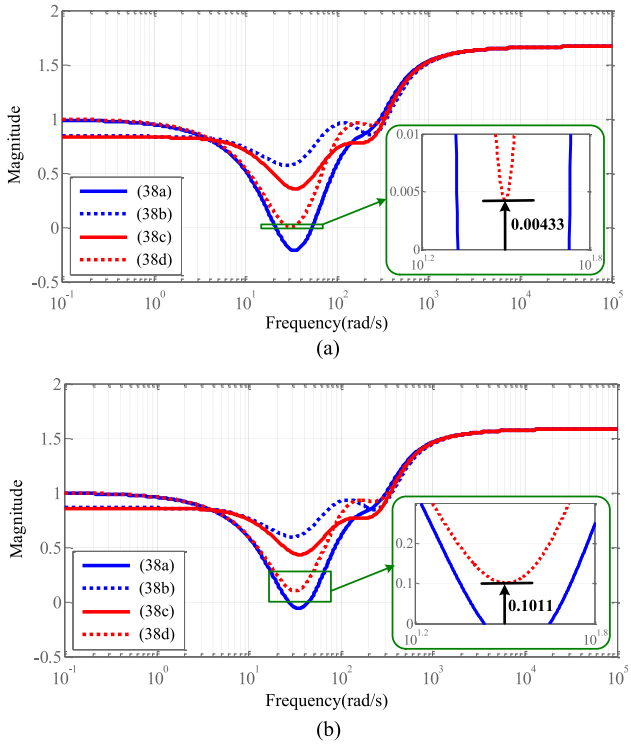

Fig. 13. Stability analyses with the FRBC when R_{S} changes. (a) $R_{\mathrm{S}} = 0.3\ \Omega$ (increasing), eight vehicles accessed to the grid (Case 2a): stable. (b) $R_{\mathrm{S}} = 0.1\ \Omega$ (decreasing), seven vehicles accessed to the grid (Case 2b): stable.

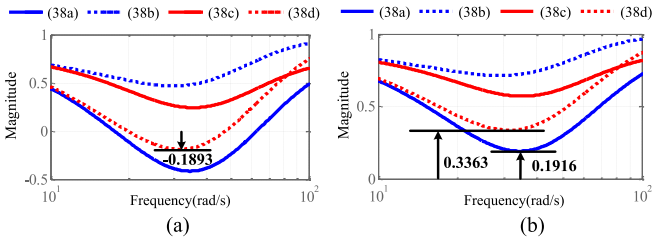

Fig. 14. Stability analyses with the FRBC when L_{S} changes. (a) $L_{\mathrm{S}} = 8\ \mathrm{mH}$ (increasing), seven vehicles accessed to the grid (Case 3a): unstable. (b) $L_{\mathrm{S}} = 4\ \mathrm{mH}$ (decreasing), eight vehicles accessed to the grid (Case 3b): stable.

influence is very small for the variation of the lowest point of the red dotted line is less than 0.02 when R_{S} changes by 50%.

With the value of L_{S} changing under Case 1, the stability analyses are also carried out in Fig. 14. The later stability analysis figures only display the important region around the lower values of the lines in the magnitude–frequency diagram for clear and easy understanding. It is indicated that the increase of L_{S} would lead to instability by comparing Fig. 12 with Fig. 14.

The percentage change of L_{S} is 33%, which is smaller than that of R_{S}. However, in Fig. 14(a), the lowest point of the red dotted line changes from 0.115 to -0.1893 compared to Fig. 12(b), and the lowest point of the red dotted line in Fig. 14(b) changes from -0.0115 to 0.3363 compared to Fig. 12(c). The variation of the red dotted line when L_{S} changes is much larger than that when R_{S} changes. It is clear that the impact on the

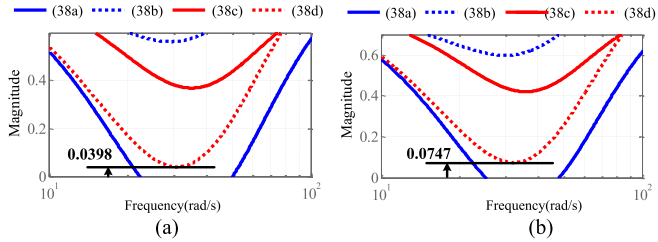

Fig. 15. Stability analyses with the FRBC when R_{n} changes. (a) $R_{\mathrm{n}} = 0.2\ \Omega$ (increasing), eight vehicles accessed to the grid (Case 4a): stable. (b) $R_{\mathrm{n}} = 0.1\ \Omega$ (decreasing), seven vehicles accessed to the grid (Case 4b): stable.

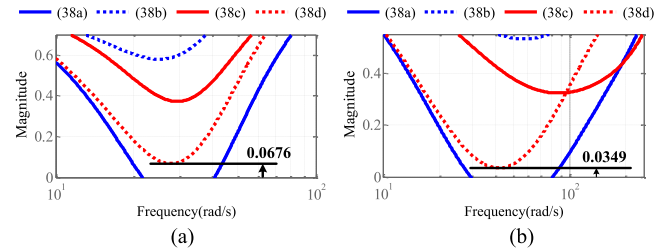

Fig. 16. Stability analyses with the FRBC when L_{n} changes. (a) $L_{\mathrm{n}} = 7\ \mathrm{mH}$ (increasing), seven vehicles accessed to the grid (Case 5a): stable. (b) $L_{\mathrm{n}} = 3\ \mathrm{mH}$ (decreasing), eight vehicles accessed to the grid (Case 5b): stable.

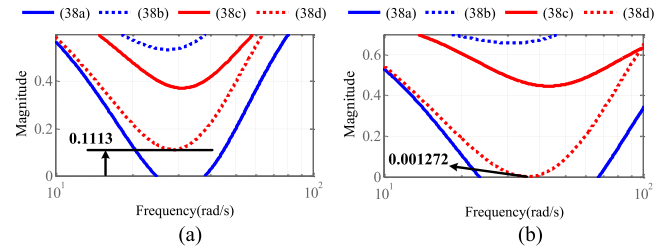

Fig. 17. Stability analyses with the FRBC when C_{d} changes. (a) $C_{\mathrm{d}} = 12\ \mathrm{mF}$ (increasing), seven vehicles accessed to the grid (Case 6a): stable. (b) $C_{\mathrm{d}} = 6\ \mathrm{mF}$ (decreasing), eight vehicles accessed to the grid (Case 6b): stable.

stability of L_{S} is much bigger than that of R_{S} although the impact trends of them are opposite. Hence, the impact of R_{S} can be ignored in contrast to L_{S}. The longer the traction network is, the more likely LFO is to occur.

2) Influence of Vehicle Parameters: In the vehicles, according to (12), (15), (17), and (19)–(22), the possible impact factors of $\boldsymbol{Y}_{\mathrm{L}dq}$ are the electrical parameters R_{n}, L_{n}, C_{d}, and the PI controller parameters K_{UP}, K_{UI}, K_{IP}, K_{II}. Here are given the detailed analyses when these parameters vary.

The stability analyses with FRBC when R_{n}, L_{n}, and C_{d} changes are presented respectively in Figs. 15–17. In Fig. 15(a), the V2G system with eight vehicles accessed becomes stable when R_{n} increases in contrast to Fig. 12(c). In Fig. 15(b), the V2G system with seven vehicles accessed tends to be unstable when R_{n} decreases in contrast to Fig. 12(b), because the lowest point of the red dotted line moves from 0.115 to 0.0747. It is indicated that the larger R_{n} benefits to the stability of the V2G system. In Fig. 16(a), the increase of L_{n} makes the lowest point

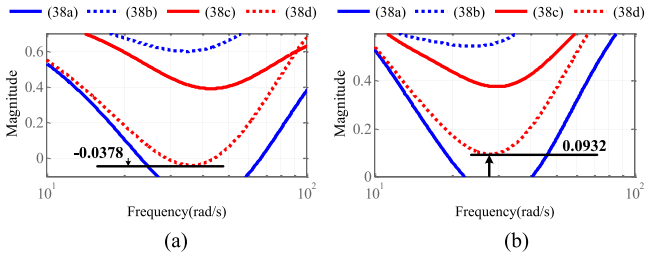

Fig. 18. Stability analyses with the FRBC when K_{UP} changes. (a) $K_{\mathrm{UP}}=1$ (increasing), seven vehicles accessed to the grid (Case 7a): unstable. (b) $K_{\mathrm{UP}}=0.1$ (decreasing), eight vehicles accessed to the grid (Case 7b): stable.

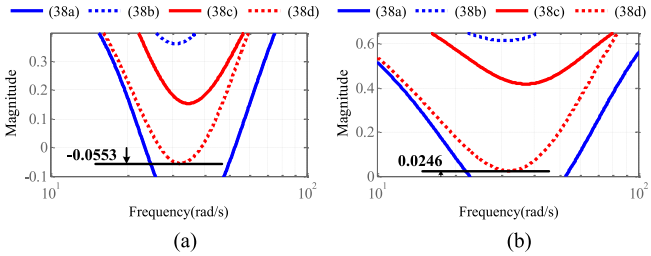

Fig. 19. Stability analyses with the FRBC when K_{UI} changes. (a) $K_{\mathrm{UI}}=7$ (increasing), seven vehicles accessed to the grid (Case 8a): unstable. (b) $K_{\mathrm{UI}}=1$ (decreasing), eight vehicles accessed to the grid (Case 8b): stable.

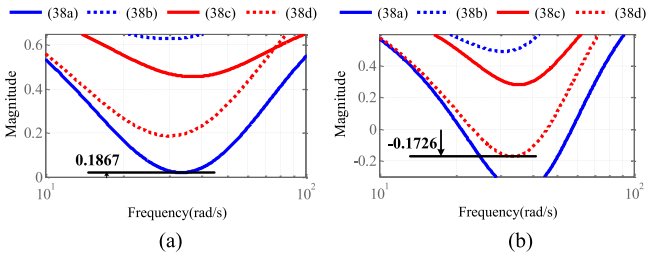

Fig. 20. Stability analyses with the FRBC when K_{IP} changes. (a) $K_{\mathrm{IP}}=2.5$ (increasing), eight vehicles accessed to the grid (Case 9a): stable. (b) $K_{\mathrm{IP}}=1.5$ (decreasing), seven vehicles accessed to the grid (Case 9b): unstable.

of the red dotted line closer to zero when seven vehicles are accessed to grid, and in Fig. 16(b), the V2G system with eight vehicles accessed becomes stable when L_{n} decreases in contrast to Fig. 12(c). Therefore, smaller L_{n} is better for the stability of the V2G system, whose influence is against R_{n}. Moreover, the variation ranges of the red dotted line are in the same order of magnitude when R_{n} and L_{n} vary, so the impacts of R_{n} and L_{n} are almost the same.

Fig. 17 displays the stability analyses when C_{d} increases and decreases. It can be found that smaller C_{d} makes the V2G system becomes stable when eight vehicles are accessed to grid in Fig. 17(b). However, the variation range of the red dotted line when C_{d} changes by 33% is less than 0.02, which manifests that the influence of C_{d} is very less compared to other parameters.

On the other hand, the parameters of PI controllers are also the impact factors of LFO. Figs. 18–21 give the stability analyses with FRBC when K_{UP}, K_{UI}, K_{IP}, K_{II} vary respectively. According to Figs. 18, 19, and 21, it can be found that the system with seven vehicles accessed to the grid becomes unstable

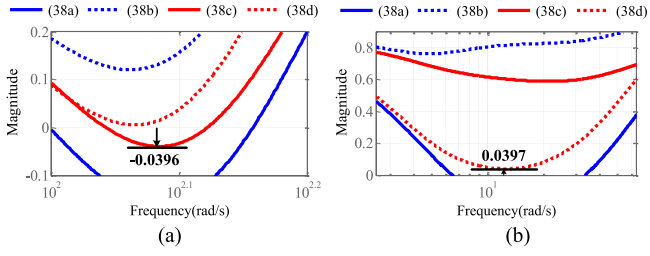

Fig. 21. Stability analyses with the FRBC when K_{II} changes. (a) $K_{\mathrm{II}}=70$ (increasing), seven vehicles accessed to the grid (Case 10a): unstable. (b) $K_{\mathrm{II}}=30$ (decreasing), eight vehicles accessed to the grid (Case 10b): stable.

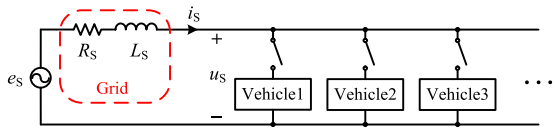

Fig. 22. Diagram of V2G system simulation model.

when K_{UP}, K_{UI} or K_{II} increases, and the system with eight vehicles accessed to the grid becomes stable when K_{UP}, K_{UI} or K_{II} decreases. Hence, larger K_{UP}, K_{UI} and K_{II} do harm to the stability of the V2G system. Moreover, Fig. 20 shows that the system with seven vehicles accessed to the grid becomes unstable when K_{IP} decreases, and the system with eight vehicles accessed to the grid becomes stable when K_{IP} increases, which indicates that smaller K_{IP} will destabilize the V2G system.

Above all, the critical unstable numbers of vehicles of the V2G system under different cases can be obtained through stability analysis with FRBC, which are shown in Table II. To manifest the advantage of the FRBC, the SVC of (30) and NC of (31) are also used to analyze the V2G system's stability respectively. The detailed analysis process of SVC and NC is not covered in this paper, but their analysis results are presented in Table II, Section V for comparison.

IV. Time-Domain Simulation and Experiment of V2G System

To validate the mathematical model and stability analysis method proposed in this paper, the time-domain simulation of a V2G system with CRH5 EMUs accessed is realized by MATLAB/Simulink. The simulation model in Fig. 22 reserves the nonlinearity of the real V2G system. The grid is equivalent to a resistor and an inductor. Different vehicles are accessed to the grid at different times via the switches.

Through simulation, the phenomenon of LFO is reproduced. Fig. 23 shows the waveforms of grid voltage, grid current and DC voltage under Case 1. Five vehicles are accessed to the grid at the beginning. At 3 s, the sixth vehicle is put into operation, and 7 s for the seventh vehicle, 12 s for the eighth vehicle.

It is shown that the V2G system becomes unstable gradually with more and more vehicles accessed to the grid in Fig. 23(a). From the enlarged waveforms of LFO in Fig. 23(b), it can be found that the amplitude variation tendencies of grid voltage and current are opposite, and the fluctuation of DC voltage U_{dc} is synchronous with that of grid voltage U_{S}. In addition, the

TABLE II
CRITICAL UNSTABLE NUMBERS OF VEHICLES FOR LFO UNDER DIFFERENT CASES

Case No.	Parameters		Stability analysis with FRBC	Stability analysis with SVC	Stability analysis with NC	Simulation	Impact
1	See details in Table I		8	5	5	8	-
2a	Grid parameters change (based on Case 1)	R_S=0.3Ω (increasing)	9	5	5	9	R_S↑ stability↑
2b		R_S=0.1Ω(decreasing)	8	5	5	8	Not obvious
3a		L_S=8mH (increasing)	6	4	4	6	L_S↑ stability↓
3b		L_S=4mH (decreasing)	12	7	7	13	L_S↓ stability↑
4a	Vehicle electrical parameters change (based on Case 1)	R_n=0.2Ω (increasing)	9	5	5	8	Not obvious
4b		R_n=0.1Ω (decreasing)	8	5	5	8	Not obvious
5a		L_n=7mH (increasing)	8	5	5	8	Not obvious
5b		L_n=3mH (decreasing)	9	3	3	8	Not obvious
6a		C_d=12mF (increasing)	8	5	5	8	Not obvious
6b		C_d=6mF (decreasing)	9	5	5	9	C_d↓ stability↑
7a	Vehicle control parameters change (based on Case 1)	K_{UP}=1 (increasing)	7	4	4	7	K_{UP}↑ stability↓
7b		K_{UP}=0.1 (decreasing)	9	6	5	9	K_{UP}↓ stability↑
8a		K_{UI}=7 (increasing)	7	5	5	7	K_{UI}↑ stability↓
8b		K_{UI}=1 (decreasing)	9	5	5	9	K_{UI}↓ stability↑
9a		K_{IP}=2.5 (increasing)	10	5	5	10	K_{IP}↑ stability↑
9b		K_{IP}=1.5 (decreasing)	6	4	4	6	K_{IP}↓ stability↓
10a		K_{II}=70 (increasing)	7	4	4	7	K_{II}↑ stability↓
10b		K_{II}=30 (decreasing)	9	5	5	9	K_{II}↓ stability↑

phase difference between the grid voltage and current goes with the fluctuation of grid voltage, which means that there exists reactive power which causes the fluctuation of grid voltage.

Fig. 24 shows the waveforms of LFO experiment [32]. Since the experiment was carried out in the real railway at the fixed substation, and the parameters of CRH5 were determined when the vehicles were manufactured, the experimental parameters were constant, and could not be changed easily. The only controllable value was the number of vehicles. Besides, the control parameters of real vehicles were also unknown. So the experiment cannot validate the small-signal model and stability analysis method directly.

However, Fig. 24(a) and (b) shows that LFO happens when the number of vehicles increases from 5 to 6 in the experiment, and the LFO waveforms of the experiment in Fig. 24(b) and (c) show the same characteristics as those of the simulation. It indicates that the simulation can reveal the property of the real V2G system.

V. RESULTS AND DISCUSSION

The stability analysis results with different criteria and the simulation results under different cases are compared in this section, which are all given in Table II. The impacts on stability of grid parameters, vehicle electrical parameters, and vehicle control parameters are also summarized according to the stability analysis.

A. Discussion on the Stability Analysis Results of FRBC, SVC, and NC

The simulation results in Table II can reflect the actual V2G system's stability. Through the comparison among the stability analysis results with FRBC, with SVC, with NC, and the simulation results, the analysis results of SVC and NC are almost the same except those under Case 7b, but are much smaller than the simulation results. However, the analysis results of FRBC are closer to the simulation results under different cases. It is indicated that the FRBC performs better in the V2G system's stability analysis than the present SVC and NC, which is due to the different limitation on the eigenvalues of $\boldsymbol{L}_{dq}$. As introduced in Section III, the SVC, NC and FRBC are all sufficient conditions of stability. The conservatism of the criteria is determined by the area of the forbidden region. The wider the forbidden region is, the larger the conservatism is. In Fig. 9, the forbidden region of SVC and NC is the outside region of the unit circle, while in Fig. 10 the forbidden region of FRBC is the left side region of $(-1+j0)$. It is obvious that the forbidden region of FRBC is much smaller than that of SVC and NC, which means the limitation on the eigenvalues of SVC and NC is stricter than that of FRBC, so the conservatism of FRBC is smaller. For the conservatism reflects the degree of the sufficiency of the criterion, the larger conservatism of SVC and NC makes their stability analysis results farther from the simulation result.

FRBC is a sufficient condition, so its stability analysis result should have also been smaller than the simulation result.

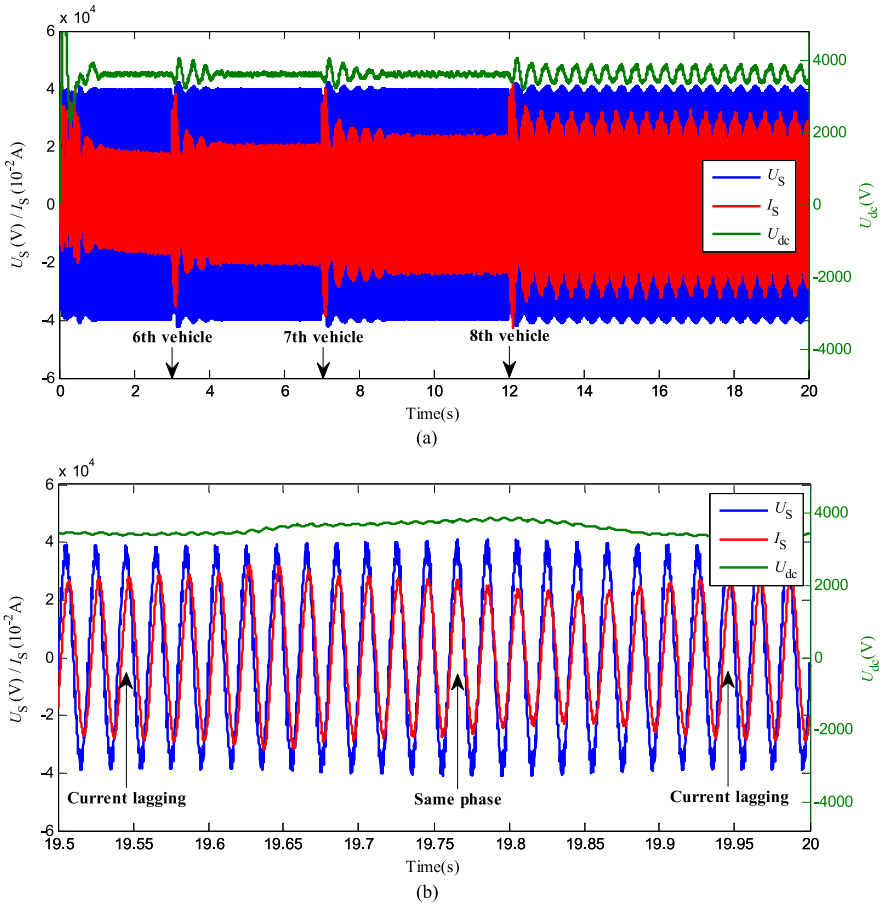

Fig. 23. LFO waveforms of grid voltage, grid current and DC voltage under Case 1. (a) LFO phenomenon with multiple vehicles accessed. (b) Enlarged waveforms of LFO.

However, only under Case 3b, the FRBC result is smaller. Under most cases, the FRBC results are equal to the simulation results. It is because the criteria analysis results and simulation results discretize the problem. One vehicle of CRH5 EMUs is equivalent to ten PWM rectifiers, and the stability analysis result is characterized by the number of vehicles, which is rounded up to an integer. The conservatism of FRBC is small enough so that the difference between its critical condition and the real critical condition may be within one vehicle. Thus most of the stability analysis results are equal to the simulation results when rounded up to the integer. For example, under Case 2a, if the critical unstable condition is characterized by the number of rectifiers, the result is 81 rectifiers, namely 8.1 vehicles. So the 8.1 vehicles need to be rounded up to 9 vehicles. But there are also some exceptions, like Case 4a and Case 5b. The FRBC cannot analyze the critical condition correctly. It may be caused by the inaccuracy of the model due to the linearization. After all, there cannot be an absolutely precise model. However, under the most cases, the FRBC results show the same tendency as the simulation on the whole, which can still verify the method is reasonable.

Since the stability analysis result is characterized by the number of vehicles, it is possible that the criterion analysis result can reflect the stability change from the number of rectifiers but cannot reflect the stability change from the visible number of vehicles when some parameters vary. For example, under Case 2a, the increase of R_S changes the simulation result from 8 to 9, but does not change the SVC and NC results, which are still 5. Apart from Case 2a, under most cases, the SVC and NC cannot reveal the stability change, while FRBC can. As a result, the FRBC can track the stability change more sensitively than SVC and NC.

According to the simulation and analysis, the impacts of the parameters are summarized in Table II. With the variation of the parameters, the movement of the four lines on the magnitude–frequency diagram of FRBC analysis can also show the impact trend, as shown in Section III-C, which is in accordance with the simulation. As for the parameters without obvious impact, not all the analysis results are convincing enough because of the inaccuracy of model. But based on the impact of the significant parameters, the stability margin of the V2G system can be considered and guaranteed by adjusting the parameters to the direction that benefits the stability.

B. Margin Design Based on FRBC

From Table II, the stability analysis of FRBC performs well, however which is just theoretical. If the FRBC is used to analyze

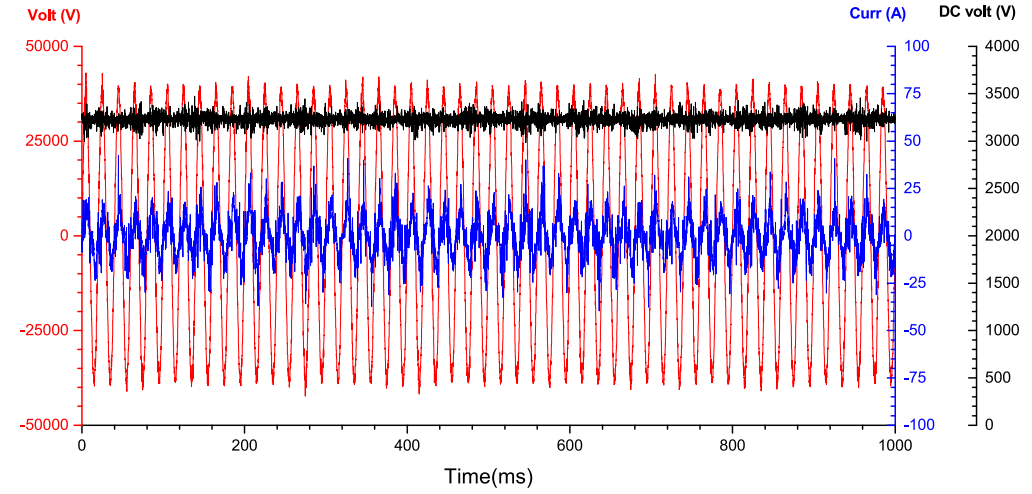

(a)

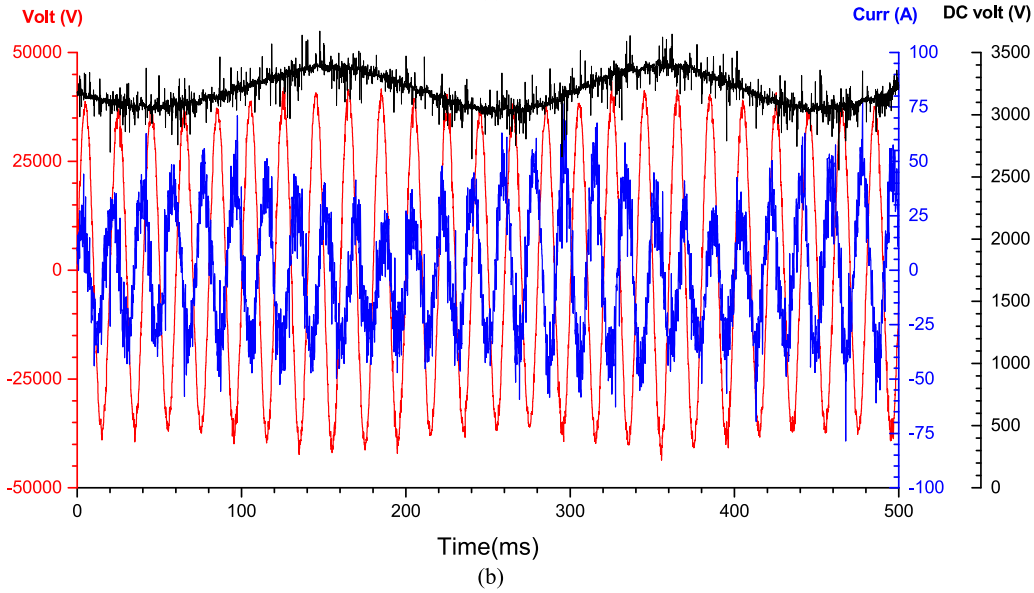

(b)

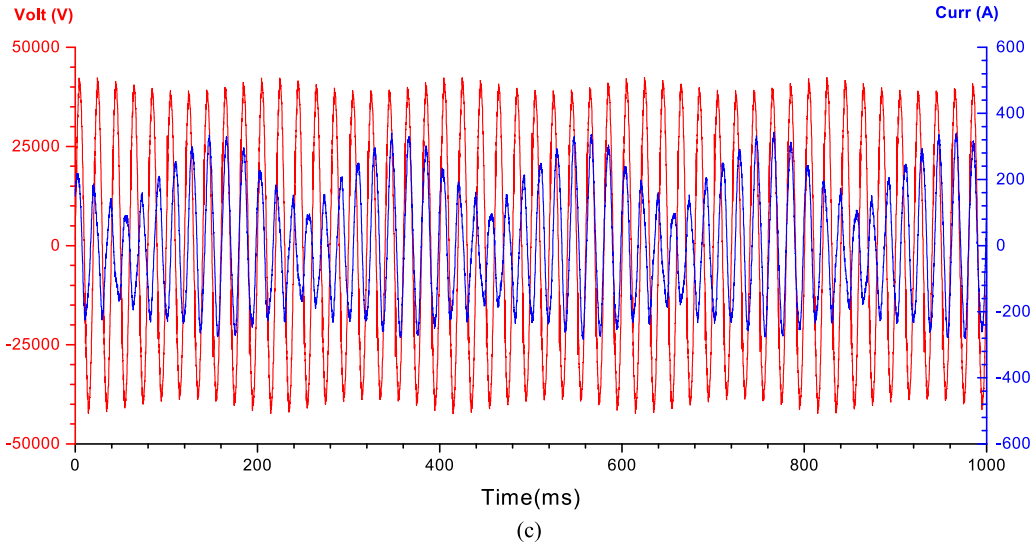

(c)

Fig. 24. Experimental waveforms. (a) Stable waveforms of grid voltage, input current of one vehicle, and DC voltage when five vehicles are accessed. (b) LFO waveforms of grid voltage, input current of one vehicle, and DC voltage when six vehicles are accessed. (c) LFO waveforms of grid voltage and grid current when six vehicles are accessed.

the stability of an actual V2G system, some difference between the theory and the reality should be taken into account. For example, the impedance of the real grid may be different from the calculated impedance, R_{S} and L_{S}, for causes like environmental conditions, wear of the wire, and so on. If the errors of calculated R_{S} and L_{S} are not considered, the FRBC may misjudge the stability near the critical condition of the V2G system. Therefore, the margin should be designed based on FRBC, which is expressed as

$$\left(\begin{cases} \mathrm{Re}\{L_{dd}\} - |L_{dq}| + 1 > M \\ \mathrm{Re}\{L_{qq}\} - |L_{qd}| + 1 > M \end{cases}\right) \cup \left(\begin{cases} \mathrm{Re}\{L_{dd}\} - |L_{qd}| + 1 > M \\ \mathrm{Re}\{L_{qq}\} - |L_{dq}| + 1 > M \end{cases}\right) \tag{39}$$

where *M* is a proper positive number to show the margin. For the precise error of the calculated impedance is uncertain, the value of *M* cannot be determined quantitatively here, but it can be adjusted to an appropriate value according to the specific actual system.

VI. Conclusion

This paper analyzes the LFO problem in the V2G system by mathematical modeling, stability analysis and simulation from the perspective of the whole cascade V2G system. A generalized *dq*-decoupled small-signal model of single-phase PWM rectifier in the vehicle is derived, and a novel stability analysis criterion based on forbidden region is put forward aiming at the V2G system stability. Through the stability analysis on a cascade V2G system and the simulation verification, some conclusions can be drawn as follows.

1) The derived mathematical model of the V2G system is reasonable and precise enough for the analysis of LFO about the significant parameters' impact. And the *dq*-decoupled small-signal model of single-phase PWM rectifier in the vehicle is a generalized one, which can be used for other *dq*-decoupled single-phase PWM rectifiers with different controls.
2) The proposed FRBC is a promotion of MISC for MIMO cascade systems. It can be used in cascade systems with either high or low power factor. In contrast to SVC and NC, it has less conservatism, and provides more accurate LFO analysis result in the V2G system. Besides, the FRBC contributes to the stability analysis of other *dq*-decoupled MIMO cascade systems.
3) Larger L_{S} and smaller R_{S} may cause LFO, but the impact of L_{S} is much bigger than that of R_{S}. Thus, as the length of traction network increases, the grid impedance is larger and more likely to result in LFO.
4) As for vehicle parameters, the influences of R_{n}, L_{n}, and C_{d} are not obvious. The control parameters are more significant, and larger K_{UP}, K_{UI}, K_{II}, smaller K_{IP} would lead to LFO.

This paper contributes to the stability analysis of complicated cascade systems with power electronic converters accessed. And the conclusions can provide design guidance for the V2G system to restrain LFO.

References

[1] Shanghai Nanxiang Switch Station, Test report of catenary voltage and current of CRH1067, 2010.

[2] H. Wang and M. Wu, "Test and analysis on low frequency oscillation of traction power system voltage caused by EMUs," presented at the 27th 648 China College Power System Automation Annual Conf., Qinhuangdao, China, Oct. 14–17, 2011.

[3] Q. Li, "Vehicle- grid electrical matching in electrified railways," *Electr. Railway*, vol. 3, pp. 13–16, 2014.

[4] S. Menth, M. Meyer, and Wettingen, "Low frequency power oscillations in electric railway systems," *Eb—Elektrische Bahnen*, vol. 104, no. 5, pp. 216–221, 2006.

[5] Q. Zheng, "A probe on causes and solutions of the HXD1 AC locomotive's resonance," *The World Inverters*, vol. 2, pp. 40–44, 2009.

[6] C. Heising, M. Oettmeier, V. Staudt, A. Steimel, and S. Danielsen, "Improvement of low-frequency railway power system stability using an advanced multivariable control concept," in *Proc. IEEE Ind. Electron.*, 2009, pp. 560–565.

[7] C. Heising, F. Jie, R. Bartelt, V. Staudt, and A. Steimel, "Modelling of rotary converter in electrical railway traction power-systems for stability analysis," in *Proc. Electr. Syst. Aircraft, Railway Ship Propulsion*, 2010, pp. 1–6.

[8] J. Suarez, P. Ladoux, N. Roux, H. Caron, and E. Guillame, "Measurement of locomotive input admittance to analyse low frequency instability on AC rail networks," in *Proc. Int. Symp. Power Electron., Electr. Drives, Autom. Motion*, 2014, pp. 790–795.

[9] H. Wang, M. Wu, and J. Sun, "Analysis of low-frequency oscillation in electric railways based on small-signal modeling of vehicle-grid system in dq frame," *IEEE Trans. Power Electron.*, vol. 30, no. 9, pp. 5318–5330, Sep. 2015.

[10] B. Wen, D. Boroyevich, R. Burgos, P. Mattavelli, and Z. Shen, "Small-signal stability analysis of three-phase AC systems in the presence of constant power loads based on measured d-q frame impedances," *IEEE Trans. Power Electron.*, vol. 30, no. 10, pp. 5952–5963, Oct. 2015.

[11] M. Belkhayat, "Stability criteria for AC power systems with regulated loads," Ph.D. dissertation, Purdue Univ., West Lafayette IN, USA, 1997.

[12] S. Chandrasekaran, D. Borojevic, and D. K. Lindner, "Input filter interaction in three phase AC–DC converters," in *Proc. IEEE Power Electron. Spec. Conf.*, 1999, pp. 987–992 vol. 2.

[13] F. Liu, J. Liu, H. Zhang, D. Xue, S. U. Hasan, and L. Zhou, "Modified norm type stability criterion for cascade AC system," in *Proc. IEEE Energy Convers. Congr. Expo.*, 2013, pp. 442–447.

[14] H. Mao, D. Boroyevich, and F. C. Y. Lee, "Novel reduced-order small-signal model of a three-phase PWM rectifier and its application in control design and system analysis," *IEEE Trans. Power Electron.*, vol. 13, no. 3, pp. 511–521, May 1998.

[15] R. Burgos, D. Boroyevich, F. Wang, K. Karimi, and G. Francis, "On the AC stability of high power factor three-phase rectifiers," in *Proc. IEEE Energy Convers. Congr. Expo.*, 2010, pp. 2047–2054.

[16] R. Burgos, D. Boroyevich, F. Wang, K. Karimi, and G. Francis, "AC stability of high power factor multi-pulse rectifiers," in *Proc. IEEE Energy Convers. Congr. Expo.*, 2011, pp. 3758–3765.

[17] B. Wen, D. Boroyevich, R. Burgos, P. Mattavelli, and S. Zhiyu, "D-Q impedance specification for balanced three-phase AC distributed power system," in *Proc. IEEE Appl. Power Electron. Conf. Expo.*, 2015, pp. 2757–2771.

[18] C. M. Wildrick, F. C. Lee, B. H. Cho, and B. Choi, "A method of defining the load impedance specification for a stable distributed power system," *IEEE Trans. Power Electron.*, vol. 10, no. 3, pp. 280–285, May 1995.

[19] X. Feng, Z. Ye, K. Xing, F. C. Lee, and D. Borojevic, "Individual load impedance specification for a stable DC distributed power system," in *Proc. Appl. Power Electron. Conf. Expo.*, 1999, pp. 923–929 vol. 2.

[20] X. Feng, J. Liu, and F. C. Lee, "Impedance specifications for stable DC distributed power systems," *IEEE Trans. Power Electron.*, vol. 17, no. 2, pp. 157–162, Mar. 2002.

[21] S. D. Sudhoff, S. F. Glover, P. T. Lamm, D. H. Schmucker, and D. E. Delisle, "Admittance space stability analysis of power electronic systems," *IEEE Trans. Aerosp. Electron. Syst.*, vol. 36, no. 3, pp. 965–973, Jul. 2000.

[22] S. Vesti, T. Suntio, J. A. Oliver, R. Prieto, and J. A. Cobos, "Impedance-based stability and transient-performance assessment applying maximum peak criteria," *IEEE Trans. Power Electron.*, vol. 28, no. 5, pp. 2099–2104, May 2013.

[23] C. Xin, "An equivalent circuit derivation method of AT power supply system," *Electr. Railway*, vol. 35, no. 1, pp. 17–20, 1999.
[24] F. Wang, "Generalized method of symmetrical components and its applications," *J. Southwest Jiaotong Univ.*, vol. 4, no. 1, pp. 1–11, 1981.
[25] Q. Ma, "Study on some problems of traction power supply systems in high-speed railway," Ph.D. dissertation, Southwest Jiaotong Univ., Chengdu, China, 2013.
[26] X. Feng, *Electric Traction AC Drives and Control System*, Beijing, China: Higher Education Press, 2009.
[27] S. Danielsen, O. B. Fosso, M. Molinas, J. A. Suul, and T. Toftevaag, "Simplified models of a single-phase power electronic inverter for railway power system stability analysis—Development and evaluation," *Elect. Power Syst. Res.*, vol. 80, no. 2, pp. 204–214, 2010.
[28] C. Zhang and X. Zhang, *PWM Rectifier and its Control*, Beijing, China: China Machine Press, 2003.
[29] A. MacFarlane, "Return-difference and return-ratio matrices and their use in analysis and design of multivariable feedback control systems,"in *Proc. Institution Elect. Eng.*, vol. 117, no. 10, pp. 2037–2049, 1970.
[30] R. Middlebrook, "Input filter considerations in design and application of switching regulators," in *Proc. IEEE Ind. Appl. Soc. Annu. Meet.*, 1976, pp. 94–107.
[31] R. S. Varga, *Gersgorin and his Circles*, Berlin, Germany: Springer-Verlag, 2004.
[32] Jinan Railway Bureau, Preliminary test results of CHR5 EMUs in Qingdao EMU station, 2010.

Yicheng Liao (S'16) was born in Sichuan, China, in 1993. She received the B.S. degree in electrical engineering and its automation from Southwest Jiaotong University, Chengdu, China, in 2015, where she is currently working toward the Ph.D. degree in electrical engineering.

Her research interests include the stability analysis of vehicle-grid system in electrified railways.

Zhigang Liu (M'06–SM'16) was born in Henan, China, in 1975. He received the Ph.D. degree in power system and its automation from Southwest Jiaotong University, Chengdu, China, in 2003.

From 2003 to 2006, he was an Associate Professor with the School of Electrical Engineering, Southwest Jiaotong University. Since 2006, he has been a Full Professor with the School of Electrical Engineering, Southwest Jiaotong University. His research interests include the electrical relationship of EMU and traction, catenary and pantograph assessment of high-speed railway.

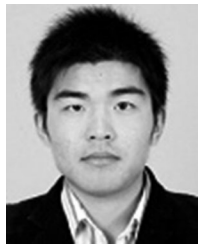

Guinan Zhang was born in Heilongjiang, China, in 1988. He received the B.S. degree in electrical engineering and its automation from Southwest Jiaotong University, Chengdu, China, in 2012, where he is currently working toward the Ph.D. degree in electrical engineering.

His research interests include the power quality analysis of traction networks and the control strategies of the electric multiple units.

Chuan Xiang was born in Yunnan, China, in 1991. He received the B.S. degree in electrical engineering and its automation from Southwest Jiaotong University, Chengdu, China, in 2014, where he is currently working toward the M.S. degree in electrical engineering.

His research interests include the control strategies of the electric multiple units.